PAPER 67 (SESSION V)

Fatigue crack propagation in cylindrical shells

Prof. W. M. CATANACH *, Jr. and Prof. F. ERDOGAN†

* Lafayette College, Easton, Pa.
† Lehigh University, Bethlehem, Pa.

Summary

Fatigue crack propagation in cylindrical shells under fluctuating internal pressure is studied. Crack propagation data are generated by pressurizing 6063-T6 and 6061-T4 aluminium cylinders containing a small initial longitudinal cut. The data are analyzed by using the stress intensity factor as the correlation parameter and introducing a modified model to account for the effect of bending. The stress intensity factor is obtained from the elastic analysis of the shell. In order to investigate the validity of the contention that the stress intensity factor may be used as the basis of comparison for crack propagation rates in structures with different geometries and loading conditions, fatigue data for 6061-T4 aluminium plates are obtained. The comparison of shell and plate results indicate that the crack growth rates in shells are slightly but consistently higher than that in plates.

Introduction

The problem of fatigue crack propagation in thin plate and shell structures is of considerable technological importance, as it relates directly, among other applications, to the design of aerospace vehicles, some ship structures and pressure vessels. In such structures, because of the unavoidable existence of stress raisers (e.g., holes, various forms of joining, material imperfections), generally the fatigue crack nucleates after a relatively small number of load cycles as compared to the total useful life of the structure. Because of this, in the past few decades, the phenomenon of fatigue crack propagation has been extensively studied *. However, these studies have dealt almost exclusively with crack growth in uniaxially loaded and centrally cracked thin plates. Thus, the two factors, the influence of which has to be studied separately, are the geometry of the structure, particularly the shell curvature, and combined load conditions, e.g., in-plane biaxial loading and simultaneous bending and extension.

In [3] the problem of fatigue crack propagation in flat plates subjected to pure bending was studied and a simple technique for the prediction of crack propagation rate for bending from that of uniaxially loaded plates was presented. The main conclusions of [3] was that, (a) in bending problem the stress intensity factor may be used effectively to analyze and correlate fatigue crack propagation data following the same procedure developed for plates under tension; (b) the plastic zone size is the

* For a review see, for example [1] and [2].

rational basis of comparison in predicting crack growth rate in plates under bending from that of the same plates under tension, and (c) for practical ranges of external loads the size of the yield zone is usually small compared with the crack length; as a result, it can be expressed in terms of stress intensity factor for both loading conditions, and hence, properly interpreted, the stress intensity factor becomes also a basis of comparison in predicting crack growth characteristics for one loading condition from that of another.

With the exception of reference [4], the influence of shell curvature on fatigue crack propagation rates has not been studied in detail, partly because the theoretical solutions for cracked shells have been available only very recently [5-7], and partly because of the (untested) assumption that a flat plate subjected to plane loads equal to the membrane stresses in the shell may have a fatigue behavior which is sufficiently close to that of the shell. Hence, the main objective of this paper is to study the effect of shell curvature on the propagation rate of fatigue cracks. Because of its simplicity and rather successful applications to flat plates, the stress intensity factor is used as a correlation parameter to analyze the experimental results and to compare them with results obtained for flat plates of the same material. As test specimens 6063-T6 and 6061-T4 aluminium cylinders are used. The stress intensity factors are obtained by solving the numerically integral equations given in [5] after separating the singularities.

Crack propagation model and theoretical procedure

The basic geometry and loading condition for the problem under consideration are a relatively long cylindrical shell subjected to fluctuating internal pressure. The shell is fixed at both ends and contains a longitudinal through crack which is sealed against leakage (Fig. 1). Since the strain in the longitudinal direction ϵ_x is zero away from the ends the uncracked shell will have only the membrane stresses σ_x^∞, σ_y^∞. Thus in solving the cracked shell problem to obtain the stress intensity factors, it is sufficient to consider an infinitely long unconstrained cylindrical shell in which the only external load is the membrane load, N_y on the crack surface.

In the elastic analysis of the shell, it is assumed that the thickness-to-radius ratio is sufficiently small, so that one is justified to use the following equations derived by Marguerre [8] for shallow shells:

$$\frac{Eh}{R}\frac{\partial^2 W}{\partial X^2} + \nabla^4 F = 0$$

$$\nabla^4 W - \frac{1}{RD}\frac{\partial^2 F}{\partial X^2} = \frac{1}{D}\,9(X, Y) \qquad (1)$$

where, referring to Fig. 1, W is the displacement in the Z direction, R is the radius, h is the thickness, F is the stress function, q is the Z component of the surface traction, E is Young's modulus and D is the flexural rigidity given by

$$D = \frac{Eh^3}{12(1-\nu^2)}$$

ν being Poisson's ratio. In the usual way, the components of the bending moment M_x, M_y, M_{xy}, and transverse shear Q_x, Q_y are given in terms of W, and the membrane forces N_x, N_y, N_{xy} are given in terms of F.

Using Fourier Transforms, the solution of (1) leads to the following systems of integral equations [5]

$$\int_{-1}^{1}\sum_{1}^{2} K_{ij}(x,t)\,u_j(t)\,dt = f_i(x),\ -1 < x < 1,\ i = 1, 2 \qquad (2)$$

where u_1, u_2 are unknown and functions f_i are related to the external loads. The kernals K_{ij} have Cauchy type singularities. After separating the singular terms in K_{ij}, (2) may be expressed as

$$\int_{-1}^{1}\sum_{1}^{2} a_{ij}u_j(t)\frac{dt}{t-x} + \int_{-1}^{1}\sum_{1}^{2} k_{ij}(x,t)u_j(t)\,dt = f_i(x)$$
$$-1 < x < 1,\ i = 1, 2 \qquad (3)$$

where a_{ij} are constants depending on Poisson's ratio and the kernels k_{ij} (x, t) are bounded functions which also depend on the shell parameter $\lambda = [12(1-\nu^2)]^{1/4}a/(Rh)^{1/2}$, a being the half-crack length.

The membrane or extensional and bending components of the stress intensity factor are the linear combinations of the quantities

$$A_i = \lim_{x\to 1} u_i(x)/(1-x^2)^{1/2},\ i = 1, 2$$

and the final results may be expressed as

$$K_{es} = P_e K_e,\ K_{bs} = P_b K_e,\ K_e = \sigma_0\sqrt{a} \qquad (4)$$

where K_{es} and K_{bs} are, respectively the extensional and bending components of the stress intensity factor, ratios P_e and P_b are functions of the shell parameter λ, and σ_0 is the uniform membrane stress $N_y/h = qR/h$ which is obtained from the analysis of uncracked shell.

The formulation of the problem and derivation of (2), as well as the asymptomatic values of P_e and P_b for small values of λ will be found in

[5]. Details of the solution of (3) and evaluation of P_e and P_b will be found in [9]. [6] gives quantities equivalent to P_e and P_b in graphical form, which are also given in [7] as a limiting case of a problem dealing with a circumferentially stiffened shell containing a longitudinal crack.

It should be noted that the solutions mentioned above are based on an 8th order shell theory in which, in addition to N_y, N_{xy} and M_y, the effective transverse shear V_y is specified on the boundary. This is equivalent to the Kirchhoff Theory of plates and would not be expected to give the correct stresses near the boundary. It is known that a 6th order theory for plates, which accounts for all the physical boundary conditions, gives an angular distribution for the stresses near the crack tip which is, unlike the results of Kirchhoff Theory, the same as that obtained for plane problems; however, the stress intensity factor for this higher order theory turns out to be dependent on the plate thickness [10]. This implies that to obtain the correct stress intensity factor in the shells, formulation of a 10th order shallow shell theory and its solutions are needed. One may argue that since the present solutions evaluate stress intensity factor ratios, and these ratios would not be expected to vary significantly if a higher order shell theory is used, and also for practical ranges of λ, P_b is within 6% of P_e, implying that bending is not really an important factor, the errors resulting from these solutions would be negligible. However, the fact that the governing equations for the shells are coupled with respect to quantities giving membrane and bending components of the stresses and that in the 6th order plate theory the stress intensity factor is not independent of the plate thickness, leads one to be somewhat more cautious about the validity of this conclusion and makes the studies to obtain a higher order solution a worthwhile undertaking.

With a technique available to calculate the stress intensity factors in the shell for a given geometry and loading condition, one needs a fatigue crack propagation model which is essentially based on the elastic solution to analyse the fatigue results. Assuming that the curvature effect is taken care of by evaluating the stress intensity factor ratios, here the characteristic feature of the phenomenon which will have to be considered in formulating a model is the generality of the loading condition, namely that the loads fluctuate about a mean value, both extension and bending are present simultaneously and the shell is stressed also parallel to the crack. The following model which will be adopted in this study is a slightly modified version of that given in [11]:

$$\frac{da}{dn} = B(1+\Omega)^{2\alpha_1}\left(K_{res} + \frac{K_{rbs}}{2}\right)^{2(\alpha_1+\alpha_2)} \tag{5}$$

$$\Omega = (\sigma_{0\,max} + \sigma_{0\,min})/(\sigma_{0\,max} - \sigma_{0\,min})$$

where K_{res} and K_{rbs} are the range values of respectively, the extensional and bending components of the stress intensity factor in the shell, σ_0 is the membrane stress in Y direction for uncracked shell, α_1, α_2 and B are positive (material) constants. In limiting cases when K_{rbs} or K_{res} is zero, (5) reduces to the models used for the extension and bending of plates. Since the crack growth model (5) uses the stress intensity factor as the correlation parameter, it assumes that the component of the external load parallel to the crack has no influence on the propagation rate.

Experimental procedure and the fatigue results

The main part of the experimental work was devoted to the generation of fatigue crack propagation data in cylindrical shells subjected to fluctuating internal pressure. The specimens were 6063-T6 and 6061-T4 aluminium cylinders. The nominal dimensions of the 6063 cylinders were $2R = 8$ in, $h = 0{\cdot}072$ in and those of the 6061 cylinders were $2R = 3{\cdot}5$ in, $h = 0{\cdot}022$ in. An initial saw cut of approximately 0·2 in long and 0·011 in wide was introduced to the cylinders. The ends of the cuts were further sharpened to reduce the crack initiation time. A hydraulic unit was used for pressurization. The sealing was accomplished by cementing a $2 \times 3 \times 0{\cdot}003$ in steel shim to a vinyl patch which was placed inside the cylinder. The shim was coated with a thin layer of graphite to eliminate any possible effect of friction between the shim and the specimen. To reduce the oil volume, the cylinder was mounted on a steel pipe providing a radial clearance of approximately 0·1 in.

The pressurization unit was calibrated with a dead weight tester and the test pressure was also verified and monitored through the strain gages applied on the cylinder at various locations outside the perturbation zone of the crack and the end clamps. In all tests the maximum stress in the cylinder away from the crack was kept below one half of the yield stress of the material. The crack length was measured by a travelling microscope giving $2a$ vs. n, (i.e., crack length vs. the number of load cycles) in tabular form. In the analysis da/dn was obtained by differentiating the data numerically by means of a three point central difference technique.

To correlate the experimental data, the range value of the 'resultant stress intensity factor' defined in (5) was evaluated as

$$K_r = K_{res} + \frac{K_{rbs}}{2} = \left(P_e + \frac{P_b}{2}\right)\sqrt{(a)}\,(\sigma_{0\,max} - \sigma_{0\,min})/2 \tag{6}$$

where the stress intensity factor ratios P_e and P_b are obtained from the elastic solution for the appropriate value of the shell parameter λ.

Thus, to obtain the constants B, α_1 and α_2 and to verify the validity of the model given by (5), da/dn was plotted against K_r for each value of Ω. Noting that $B(1 + \Omega)^{2\alpha_1}$ is constant for a fixed Ω, after a least square straight-line fit, these plots give the values of the exponent $2(\alpha_1 + \alpha_2)$. Results are given in Table 1. The last column in this table shows the correlation coefficient r for the least square straight-line fit of log (da/dn) vs. log K_r. The closeness of r to unity indicates that within the ranges covered by (da/dn) and K_r, the power relationship assumed in (5) is justified.

The values of $B(1 + \Omega)^{2\alpha_1}$ given in Table 1 are obtained by using a common value for the exponent $2(\alpha_1 + \alpha_2) = 3{\cdot}85$ which is evaluated from a least square straight line fit to the entire data in $\log(da/dn)$ vs. log K_r plot.

The constants B and α_1 are then obtained by plotting $B(1 + \Omega)^{2\alpha_1}$ against $(1 + \Omega)$ on log-log scale. Thus, for example, for the fatigue crack propagation rate in 6063-T6 aluminium shells, the following empirical relation is obtained

$$\frac{da}{dn} = 1{\cdot}068 \times 10^{-19}(1 + \Omega)^{0{\cdot}753} K_r^{3{\cdot}85} \tag{7}$$

Figure 2 shows a typical result for an individual 6063-T6 shell in which da/dn is plotted against K_r. Figure 3 shows the combined data for three levels of mean-to-range pressure ratio Ω. The slight shift to the left observed in this plot for increasing Ω is characteristic of flat plate fatigue experiments. Figure 4 shows similar results for twelve 6061-T4 aluminium cylinders *. These cylinders had the dimensions $2R = 3{\cdot}5$ in, $h = 0{\cdot}22$ in. The average of the exponents for these shells was $2(\alpha_1 + \alpha_2)_{av} = 4{\cdot}05$. Figure 5 shows the flat plate results for 6061-T4 aluminium of approximately the same thickness. Experiments for the shells and plates were obtained under similar laboratory conditions. The approximate mean of the plate results is also shown in Fig. 4 for comparison. Again for the purpose of comparison, the means of the 6063-T6 and 6061-T4 shell results are plotted in Fig. 6 with the means of 2024-T3 and 7075-T6 aluminium plates. The data for these plates were reported in [12] and analyzed in [13]; in the tests Ω varied between 1·13 and 4·8.

Strain measurements ahead of the crack

For a partial verification of theoretical results, static strain measurements were made ahead of the crack tip at various crack lengths using

* The data for 6061-T4 cylinders and plates were obtained by John Kibler of the Dept. of Mech. Engrg., Lehigh University, Bethlehem, Pa.

$\frac{1}{16}$ in foil gages. Assuming that strains near the crack tip are the sum of the strains outside the perturbation zone of the crack given by

$$\epsilon_x^\infty = 0,\ \epsilon_y^\infty = \frac{1 - \nu^2}{E}\frac{9R}{h} \tag{8}$$

and those at the crack tip given by the leading term with $\sigma_x \cong \sigma_y$, namely

$$\epsilon_y^l \cong \frac{1 + \nu}{E} P \frac{9R}{h}\sqrt{\frac{a}{2r}},\quad P = P_e + P_b \tag{9}$$

we may write

$$\epsilon_y \cong \epsilon_y^\infty\left(1 + \frac{P}{1 + \nu}\sqrt{\frac{a}{2r}}\right) \tag{10}$$

For a relatively low stress state away from the crack *, for which the effect of plastic deformations around the crack tip is expected to be small, the experimental results and equation (10) are shown in Fig. 7. The agreement is obviously unsatisfactory. The difference may be due partly to the finite gage length and the effect of plastic deformations, and partly to the fact that the singular term alone, (i.e., (9)) does not correctly predict the perturbed strains caused by the crack in a homogeneous strain field. In the shell, even though the far field perturbed solution is not available, a reasonable estimate for it may be obtained by drawing an analogy with a flat plate and introducing a factor $T(r)$ which appears in the exact solution of plane problems. From the solution of a cracked plate subjected to a pressure σ_0 on the crack surface, we have

$$\epsilon_y^p = \frac{1 - \nu}{E}\sigma_0\sqrt{\frac{a}{2r}}\,T(r),\quad T(r) = \sqrt{\frac{2r}{a}}\left(\frac{a + r}{\sqrt{[r(2a + r)]}} - 1\right) \tag{11}$$

For small r, $T = 1$ and (11) gives the plate equivalent of (9). Thus, if we now modify (10) by multiplying the perturbed solution by T, we obtain

$$\epsilon_y \cong \epsilon_y^\infty\left(1 + \frac{P}{1 + \nu}\sqrt{\frac{a}{2r}}\,T(r)\right) \tag{12}$$

Comparison of (12) and the experimental results are shown in Fig. 8. The agreement is now satisfactory. However, it should be noted that at

* These experiments were performed on 6063-T6 cylinders with $\sigma_{y\,max}/\sigma_{yield} \cong 0{\cdot}1$ and $r = 0{\cdot}05$-$0{\cdot}08$ in.

higher stress levels (12) underestimates the strains, meaning that the effect of plastic deformations is no longer negligible.

Discussion and conclusions

As in most plate experiements, crack propagation in a shell started as a flat (plane strain) fracture changing to a shear fracture when a certain value of the stress intensity factor K_r, was exceeded. In [14], for 2024-T3 and 7075-T6 aluminium plates this transition range of K_r was found to be 3540 ∓ 1770 lb/in$^{3/2}$. The results for some of the 6063-T6 cylinders are shown on Table 2. As the transition usually initiated on the outer surface, the range values of the stress intensity factor given in Table 2 were obtained from $K_r = (P_b + P_e) K_{re}$. The transition values of K_r for the cylinders fall within the interval of 3440 ∓ 1220 lb/in$^{3/2}$, which compares favorably with the results found in [14].

A direct attempt at the verification of the theoretical solution was made by measuring strains ahead of the crack in a plate of dimensions 24 in $\times$ 12 in $\times$ $\frac{1}{8}$ in and a cylinder 20 in long 9½ in in diameter and $\frac{1}{8}$ in thick. Materials for both specimens were (Commercial) Plexiglas G. The gages in the cylinder were placed inside and outside the cylinder. The ratios of the stress intensity factors corresponding to the strain readings in the shell to those in the plate were compared with the calculated values of $P_e \mp P_b$. The tests were performed at various crack lengths. There were considerable scatter in the measured values, (largely due to the difference in properties of the plate and the shell and the steady drift in the gage readings because of the viscous effects), hence the agreement was only qualitative. Nevertheless, the fact that the stress intensity factor on the outside surface of the cylinder is greater than that on the inside (for the range $0<\lambda<3$) was experimentally verified.

Following the standard procedure, da/dn is plotted in Figs. 3-5 against the range value of stress intensity factor for all values of the ratio $\Omega = K_m/K_r$. Hence, these figures show a relatively wide scatter band. However, this band narrows if the test data for various values of Ω are separated. This may be seen from Figs. 3 and 5.

In conclusion it may be remarked that the stress intensity factor obtained from the elastic solution seems to be an effective correlation parameter in shells as well as in plates in analyzing the fatigue crack propagation results. However, in using this factor as a basis of comparison, that is, for example, in predicting crack propagation rates for shells from that for flat plates of the same material, some caution is necessary. Comparison of shell and plate results given in Figs. 4 and 5 for 6061-T4 aluminium indicates that there is a certain shift in the data, that is, the growth rates for shells seems to be somewhat higher than those for plates. This may be due to two factors, both of which require further study.

First is the approximate nature of the calculated stress intensity factors in shells because of the assumption of Kirchhoff type boundary conditions. The second and perhaps a more important factor in this case is that in the analysis of the shell results the effect of the uniform stress component parallel to and away from the crack, σ_x^∞ was ignored which, unlike the plate experiments, was not zero. The crack propagation model (5) used in this study is based on the size of the plastic zone and magnitude of the plastic strains around the crack tip (see, [12]). Even though σ_x^∞ does not have any effect on the stress intensity factor, its influence on the plastic deformations around the crack tip, and hence, on the crack propagation rate may not be negligible.

Acknowledgment

This work was supported by the National Aeronautics and Space Administration under Grant NGR 39-007-011.

References

1. SCHIJVE, J. 'Significance of fatigue crack in micro-range and macro-range', in *Fatigue Crack Propagation. ASTM STP-415*, p. 415, 1967.
2. PARIS, P. C. and ERDOGAN, F. 'A critical analysis of crack propagation laws', *J. Basic Engineering, Trans. ASME*, vol. 85, p. 528, 1963.
3. ERDOGAN, F. and ROBERTS, R. 'A comparative study of crack propagation in plates under extension and bending', *Proc. 1st Int. Conf. on Fracture*, p. 341. 1965.
4. CRICHLOW, W. J. and WELLS, R. H. 'Crack propagation and residual static strength of fatigue-cracked titanium and steel cylinders', in *Fatigue Crack Propagation, ASTM STP-415*, p. 25, 1967.
5. FOLIAS, E. S. 'An axial crack in pressurized cylindrical shell', *Int. J. Fracture Mechanics*, vol. 1, p. 104, 1965.
6. COPLEY, L. G. 'A longitudinal crack in a cylindrical shell', Ph.D. Thesis, Harvard University, 1965.
7. DUNCAN, M. E. and SANDERS, Jr. J. L. 'The effect of a ring stiffener on the stress in a cylindrical shell with a longitudinal crack', Harvard University Report SM-13, prepared for the National Aeronautics and Space Administration, 1967.
8. MARGUERRE, K. 'Zur Theorie der gekrümmten Platte grosser Formänderung', *Proc. 5th Congress Appl. Mech.*, p. 93, 1938.
9. CATANACH, Jr. W. M. and ERDOGAN, F. 'Fatigue crack propagation in cylindrical shells', to appear as NASA Contractor Report, 1968.
10. HARTRANFT, R. J. 'On some problems involving singularities in Reissner's theory of plate be nding' Ph.D. Thesis, Lehigh University, 1966.
11. ERDOGAN, F. 'Crack propagation theories' NASA CR-901, 1967.
12. BROEK, D. and SCHIJVE, J. 'The influence of the mean stress on the propagation of fatigue crack in aluminium alloy sheet', NLR-TR M.2111, Nat. Aerospace Laboratory, Amsterdam, 1963.
13. ROBERTS, R. and ERDOGAN, F. 'The effect of mean stress on fatigue crack propagation in plates under extension and bending', *J. Basic Engrg., Trans. ASME*, vol. 89, p. 885, 1967.
14. WILHEM, D. P. 'Investigation of cyclic crack growth transitional behavior', in *Fatigue Crack Propagation, ASTM STP-415*, p. 363, 1967.

Table 1
Results for 6063-T6 aluminium

Shell No.	Ω	$B(1+\Omega)^{2\alpha_1}$	$2(\alpha_1+\alpha_2)$	r
9	1·087	$2{\cdot}69\ 10^{-19}$	3·82	0·994
10	1·066	$6{\cdot}99\ 10^{-20}$	3·99	0·980
11	1·065	$2{\cdot}82\ 10^{-18}$	3·46	0·970
12	1·065	$1{\cdot}97\ 10^{-18}$	3·54	0·965
13	3·259	$2{\cdot}54\ 10^{-17}$	3·29	0·975
14	1·077	$1{\cdot}16\ 10^{-17}$	3·37	0·994
15	1·644	$5{\cdot}05\ 10^{-17}$	3·19	0·998
18	1·055	$4{\cdot}21\ 10^{-18}$	3·46	0·965

Table 2.
Transition from flat-to-shear fracture

	Transition initiation			Transition end		
Shell	a	K_r	da/dn	a	K_r	da/dn
9	*			0·293	4140	$1{\cdot}75\ 10^{-5}$
11	0·360	2610	$1{\cdot}8\ 10^{-6}$	0·550	3910	$8{\cdot}00\ 10^{-6}$
12	0·285	3240	$4{\cdot}2\ 10^{-6}$	0·449	3760	$1{\cdot}75\ 10^{-5}$
13	*			0·465	3300	$9{\cdot}70\ 10^{-6}$
18	0·149	2100	$1{\cdot}6\ 10^{-6}$	0·422	4520	$1{\cdot}40\ 10^{-5}$

* Not clearly definable.

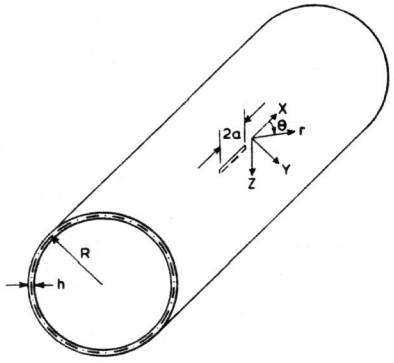

Fig. 1. Shell geometry and coordinates.

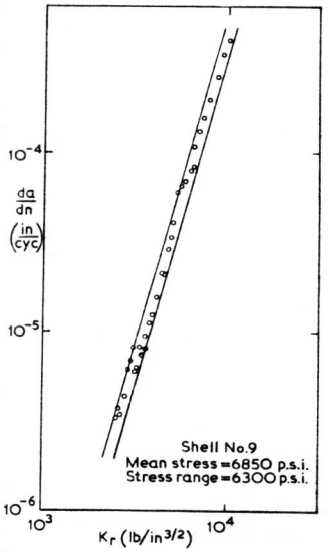

Fig. 2. Crack growth rate for an individual cylinder.

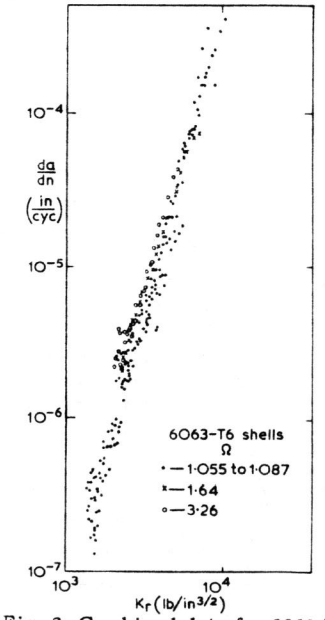

Fig. 3. Combined data for 6063-T6 aluminium cylinders.

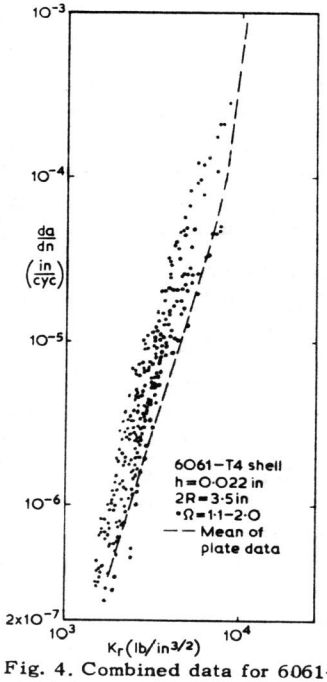

Fig. 4. Combined data for 6061-T4 aluminium cylinders.

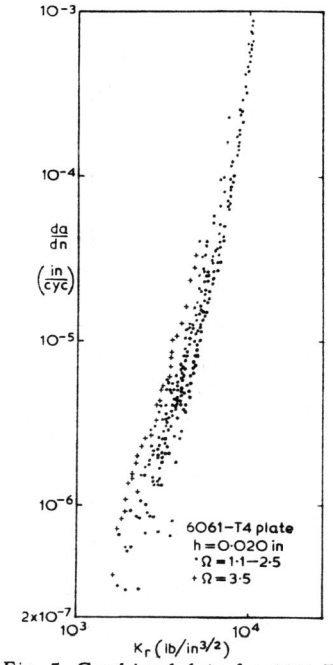

Fig. 5. Combined data for 6061-T4 aluminium plates.

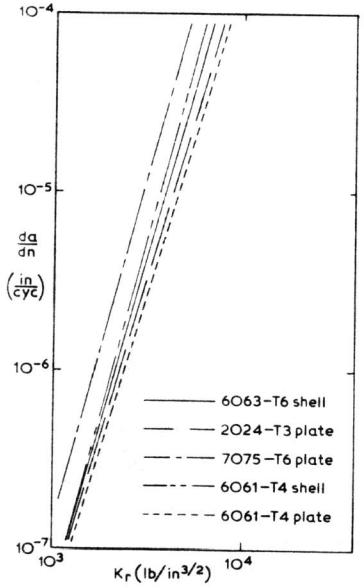

Fig. 6. Crack growth rates in various aluminium alloys.

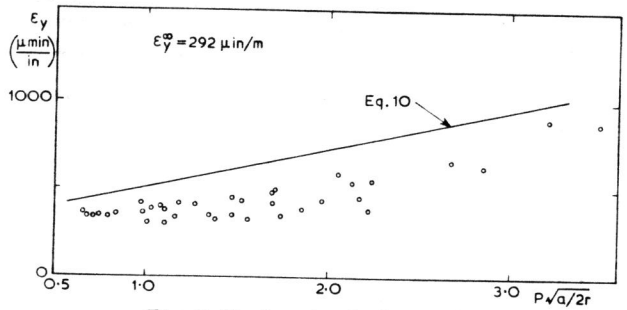

Fig. 7. Strains ahead of the crack tip.

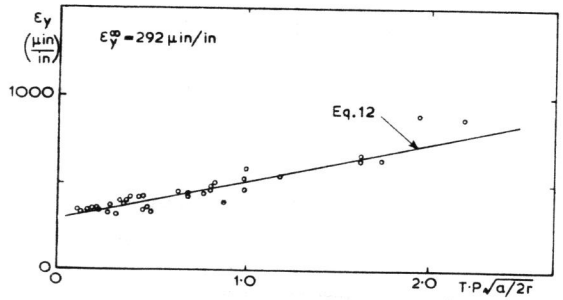

Fig. 8. Strains ahead of the crack tip.